New Synthesis Route of Lead -free Hybrid Graphene Nanoparticles

Seham K. Abdel-Aal[1,], Ahmed S. Abdel-Rahman[1] ,S. H. Ismail [2]*

[1] Physics Department, Faculty of Science, Cairo University, 12613, Giza, Egypt.
[2] Geology Department EGNC, Faculty of Science, Cairo University, 12613, Giza, Egypt.

In this work, a green and facile synthesis of a reduced graphene oxide/Cu nanoparticles hybrid Cu-rGO is presented by using extracted pure limon juice. Characterization tools confirmed the reduction of graphene oxide. Copper nanoparticles were successfully decorated over the rGO sheets with average crystallite size 34 nm. The Cu nanoparticles are uniformly distributed on graphene sheets except few aggregates. X-ray diffraction proves the formation of single cubic phase of the prepared Cu-rGO nanoparticles and reduction of graphene oxide into its reduced form. Raman spectroscopy shows its vibration modes. Morphological characterization by atomic force microscopy (AFM), scanning and transmission electron microscope (SEM) and (TEM) photos are also provided, as will as Brunauer-Emmett-Teller (BET) measurements, the pores dimensions of Cu-rGO nanohybrid may find applications in supercapacitors.

1. Introduction:

Year by year, energy demands increase and most of it comes from burning fossil fuels which causes harmful effect on the environment. This motivated the scientist all over the world to developing a new technologies regarding renewable energy. Various methods, tools and devices has been reported to generate sustainable forms of energy that is efficient and affordable [1-5].

Graphene as a 2D carbon material [6], showed intense potential for applications in high efficient supercapacitors [7-13], solar cells [14], energy [15,16], photoelectric technology [17,18] and catalysis [19-21] owing to its excellent electrical and optical properties. The graphene oxide (GO) is the main precursor for the preparation of graphene through chemical reduction or thermal annealing [22,23] or microwave assisted synthesis. Moreover, carboxyl, hydroxyl and epoxy groups as the oxygen functional groups are released [24,25]. The generation of defects on GO surface during oxidation stage acts as anchoring sites for deposition of nanoparticles of the used metal as reported [5,26,27]. Graphene-metal nanocomposites were explored and showed great potential in some catalytic reactions. Cu-rGO was used for oxidation of benzyl alcohol and other substituted

benzyl alcohol in water [28-30]. Another route is the use of Cu-rGO nano hybrid in the carbon dioxide reduction since it is the main gas produced by human activity and the main reason for greenhouse effect [5]. The synergistic effect between copper nanoparticles and graphene sheets enable potential such multifunctional applications.

The present work provides a green and fast synthetic route of Cu-rGO nanohybrid for multifunctional applications. The synthesis time took about 75 min where a simultaneous reduction of GO and $Cu(SO_4)$ by pure lemon juice takes place. The formation of Cu on the surface of graphene sheet is confirmed by X-ray diffraction XRD, Raman spectroscopy and morphological characterization was done by scanning and transmission electron microscope. The isotherm of Brunauer-Emmett-Teller (BET) is discussed.

2. Experimental Procedures:

2.1. Synthesis of Graphene oxide:

Chemicals used in the synthesis process are purchased from Sigma-Aldrich with purity exceeds 98% and used as received without further purification. Graphene oxide synthesized from graphite powder by using the Hummer's method [6] as reported in our previous work [12, 13]. Details of the synthesis summarized as follow: 5 g of graphite powder and 2.5 g of $NaNO_3$ were dispersed in 125 ml H_2SO_4 (98%) as intercalating agent and stirred for 120 min. Then to the above solution, 15 g of grinded $KMnO_4$ was added gradually. The temperature of the solution was kept under 20°C by keeping it into ice bath where the resulting solution had deep oily green color. Then the mixture was stirred at 35-37 °C for 90 min. The resulting solution diluted gradually by adding deionized water under vigorous stirring. The suspension is treated further by adding 30 ml of 30% H_2O_2 solution and 350 ml of distilled water. A bright orange color of graphene oxide suspension was appeared after adding the peroxide solution. The resulting suspension was washed several times with deionized water until the pH of the solution became neutral. The solution was dried in temperature not exceeds 60°C, ground and finally the silver brown powder of graphene oxide was ready to use. Fig. (1) show that the three stages of preparation of graphene oxide [12].

2.2. Synthesis of Cu-rGO/ Nanohybrid

100 ml of lemons juice were add to 100 ml of deionized water and heated to 70ºC for 45 min. The solution was filtered and 25 ml of extracted solution was added to 0.30 mg of graphene oxide and 0.3 M of $CuSO_4$ solution. The solution was stirred for 1 h at 60ºC then alternated by a probe sonicator of 75% amplitude and 0.5% cycle for 1 h until the black rose color appeared. The precipitate was washed using deionized water several times and then centrifuged at 14000 rpm

for 30 min. Finally, the precipitate was dried using oven at 40ºC. The powder of Cu-rGO nanohybrid was ready for characterization.

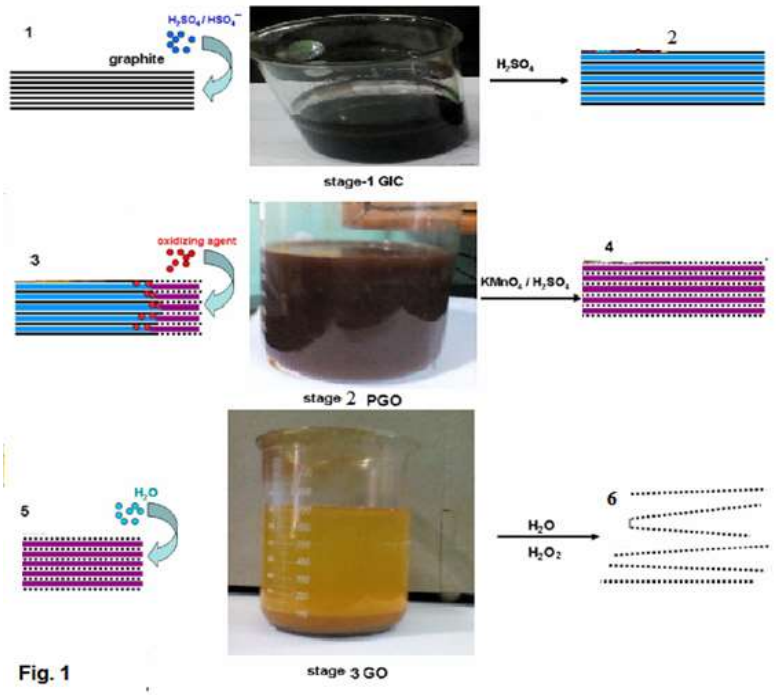

Fig. (1): Steps of preparation of graphene oxide from graphite.

2.3. Characterization

The X-ray powder diffraction (XRD) data are collected using a computer controlled Bruker (D 8 discover) diffractometer with CuKα radiation k = 1.54056 Å. The measuring range from 5º to 100º and the instrumental resolution was 0.004– 0.005º. Data collected in step-scan mode with steps of 0.02º. Morphology of the produced nanohybrid investigated using a scanning electron microscope (SEM) model number JSM 6510 LV JEOL and transmission electron microscope (TEM) model number JEM 2100 JEOL. A computer controlled Raman spectra between 100 cm^{-1} to 3000 cm^{-1} were obtained on an HORIBA JOBINYVON. The atomic force microscopy (AFM) was obtained on AFM-Agilent Technologies. The specific surface area was obtained using BET measurements on NOVAtouch, and the data of pore diameter were calculated from the Barrett-Joyner-Halenda (BJH) method.

3. Results and discussion

3.1 Structural characterization

3.1.1 X-ray diffraction

Figure (2) showed the XRD patterns of Cu-rGO nanohybrid and GO. The diffraction peaks are assigned to the cubic structure, (COD 5000216). Unlike the

XRD pattern of GO reported before [12, 13] the graphene nanohybrid of Cu-rGO doesn't show any peak at 2θ = 10° in the XRD pattern. These results ensure that the oxygen functional groups of GO are removed and GO are reduced to graphene nanosheet GNS by ascorbic acid of limon juice. The diffraction peak of GNS observed at 2θ = 24° (002) and shown in the inset figure in the XRD patterns is relatively broad and weak. The crystallinity of Cu diffraction peaks is strong and sharp as appears in the figure. Where the (111) peak intensity is 65 times more than the broad peak intensity of rGO which prove its non-crystalline nature.

The diffraction peaks of Cu-rGO are observed at 2θ 43.32°, 50.44°, 74.12°, 89.93° and 95.14° are assigned to the Cu (111), (200), (220), (311) and (222) crystal planes, respectively [5, 27]. The above results proved that Cu-rGO nanohybrid is successfully prepared.

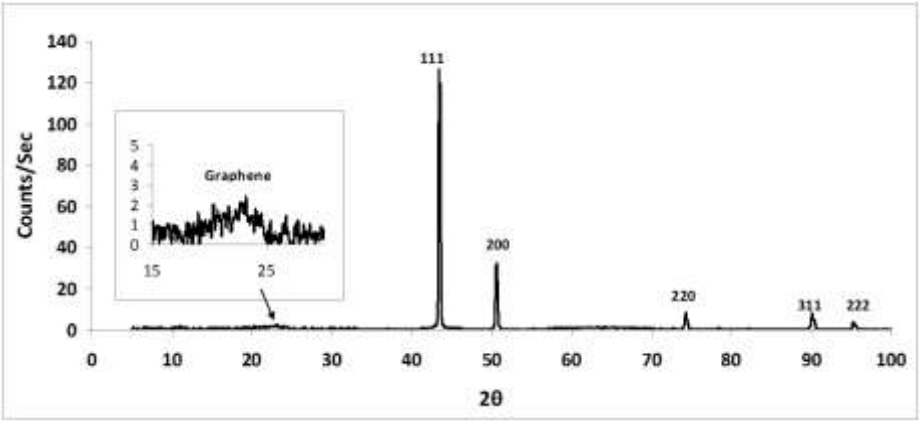

Fig. (2): X-ray diffraction of Cu-rGO nanohybrid and GO as inset.

The average crystallite size D is calculated using Debye-Scherrer's equation [12, 31] will be applied to the peak (111):

$$D = \frac{0.94\lambda}{W_f \cos\theta_D} \tag{1}$$

where W_f is the width at half maximum intensity (FWHM) of the Bragg reflection excluding instrumental broadening in radians. λ is the wavelength of the X-ray radiation (λ Cu = 1.54056 Å) and θ_D is the Bragg angle. The average crystalline size of Cu-rGO is equal to 34 nm.

The crystallites size and the average lattice strain ε can be estimated from the Williamson-Hall equation [32, 33]:

$$W = W_{strain} + W_f = 4\varepsilon \tan\theta_D + \frac{K\lambda}{D\cos\theta_D} \tag{2}$$

where W is the full width half maximum of the XRD peaks, W_{strain} is the strain broadening which is uniform in all crystallographic directions and K=0.94 is a the shape factor. When multiplying Eq. 2 by $\cos\theta_D$, it gives:

$$W\cos\theta_D = 4\varepsilon\sin\theta_D + \frac{K\lambda}{D} \quad (3)$$

Then the relation between $W\cos\theta_D$ and $4\sin\theta_D$ will be a straight line (Figure 3), the strain ε of the Cu-rGO nanohybrid is deduced from the slope of linear fitting data (gradient) whereas the D is determined from the Y-intercept ($K\lambda/D$).

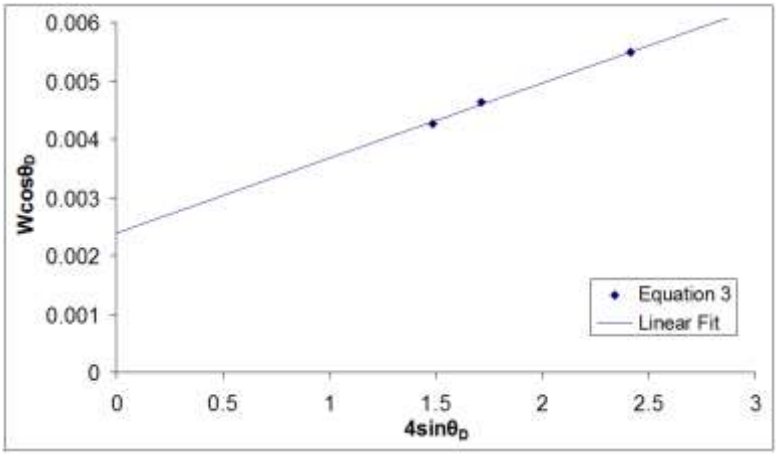

Fig. (3): Williamson-Hall equation 3 and its linear fit for Cu-rGO nanohybrid.

The estimated values of D and ε deduced by using Williamson-Hall equation are 60.7 nm and 0.0013. It is clear that, the D value as calculated using Williamson-Hall technique is higher than that obtained using Scherrer equation where Williamson-Hall equation takes into consideration all diffraction peaks and assumes the brooding of it. That is related to the crystalline size as well as the lattice strain, which is not considered in Scherrer equation [32, 33].

3.1.2. Raman Spectroscopy:

Figure (4) showed the Raman spectrum of Cu-rGO nanohybrid and GO as inset. The typical graphene peaks that containing well-recognized D and G bands are found at 1360 and 1590 cm^{-1}, respectively. The D is sharp band reflects the disordered sp^2 carbon in graphene and the G band is due to the in-plane C−C stretching [34, 33]. The Cu bands were appeared at 204 and 705 cm^{-1}. This indicates the formation of Cu-rGO nanohybrid during the synthesis process. The ratio I_D/I_G = 0.85 indicating single layer reduced graphene oxide. This is also

proved by the sharpness and position of the G band. The XRD prove the presence of graphene by broad beak centered at 2 theta equals 23 degree

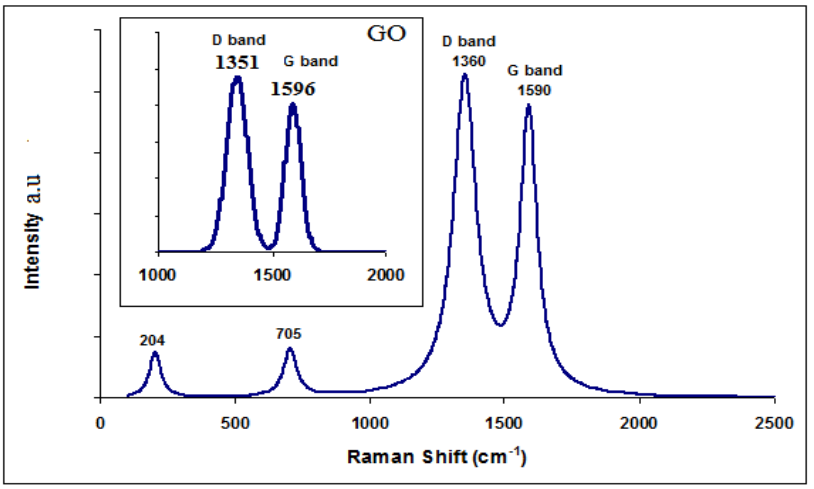

Fig. (4): Raman spectrum of Cu-rGO nanohybrid and GO as inset.

3.2. Morphological Characterization :

The SEM and TEM images of the rGO and Cu-rGO are given in Figure (5 a,b) for SEM images and Figure (6 a,b) for TEM images, respectively. The graphene sheet appears as transparent films with crumpling on the surface and the copper nano particles appears as isolated islands specially in TEM images. Obviously, the typical wrinkle structure still existed from the image of Cu-rGO, which indicates the reduction process only reduced the oxygen functional groups without destroying the layered structure. Moreover, a number of Cu nanoparticles are distributed on the surface of the rGO. It was obvious that the obtained Cu nanoparticles had a size distribution in the 40-70 nm range with an average particle size of 60 nm. The result is also consistent with the SEM image shown in Figure (5 a,b).

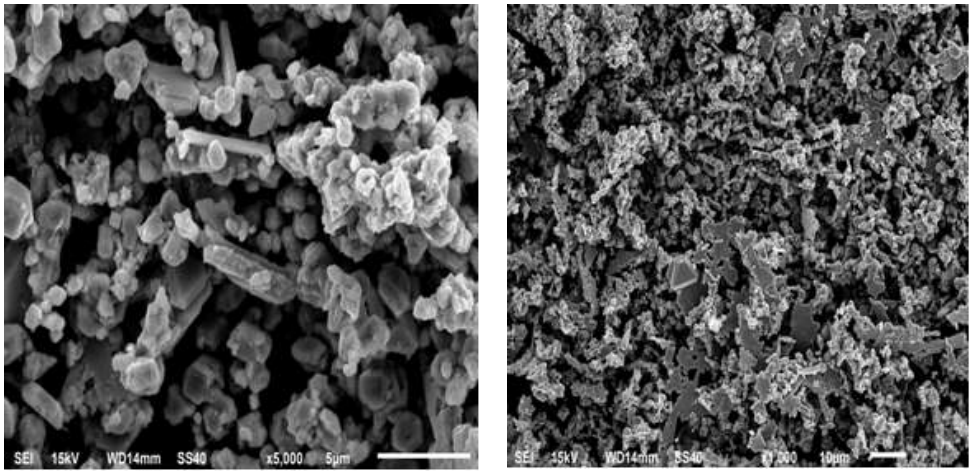

Fig. (5): (a, b). SEM images of Cu-rGO nanohybrid

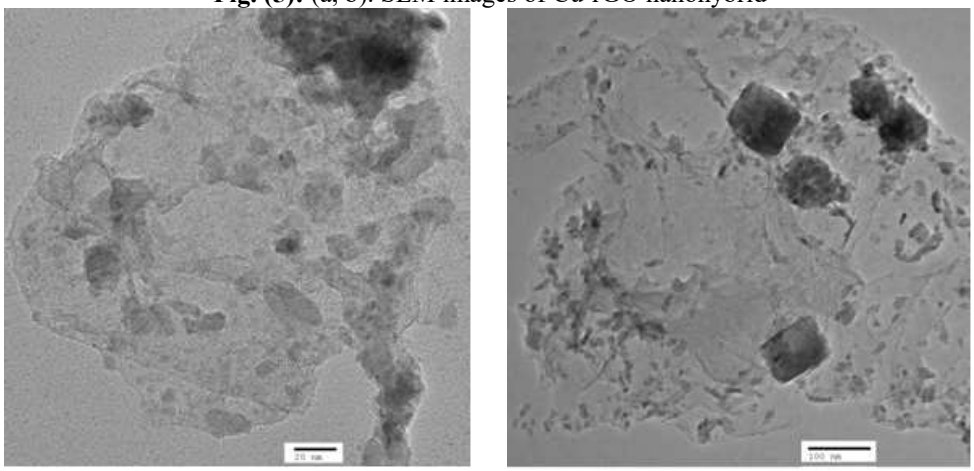

Fig. (6): (a, b). TEM images of Cu-rGO nanohybrid.

One of the AFM pictures taken to the surface of prepared Cu-rGO nanohybrid is presented in Fig. (7). The analysis of these protrusions results showed a distribution of Z_{max} and Z_{min} to be 119 nm and 16.5 nm, respectively, and the mean is around 33.5 nm. These results are consistent with that illustrated before in XRD, SEM and TEM techniques.

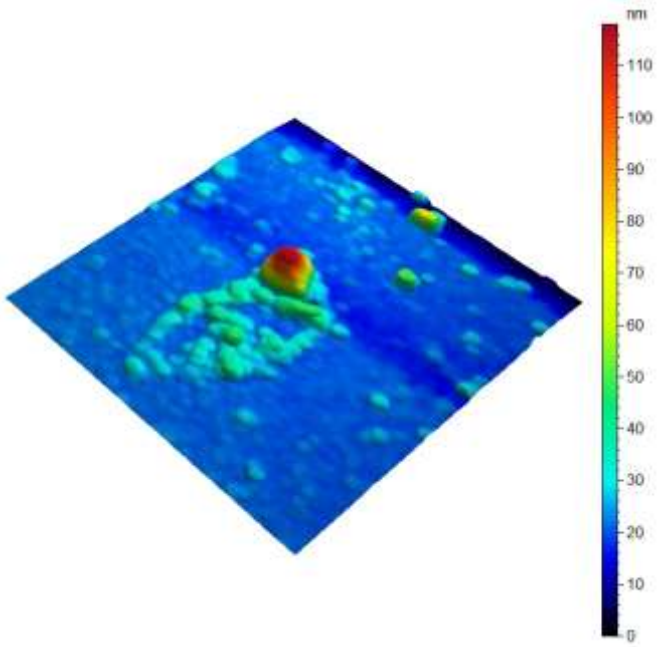

Fig. (7): The AFM surface analysis of Cu-rGO nanohybrid.

3.3. BET Measurements and BJH Analysis:

In order to evaluate the specific surface areas of the Cu-rGO nanohybrid, the N_2 adsorption-desorption isotherms analysis and BJH pore size distribution were further carried out. The Cu-rGO nanohybrid showed a very narrow hysteresis loop at the relative pressure (P/P_0) range of 0.30-0.90 (Fig. 8a), which indicated its mesoporous nature. The BET surface area is 59.17 m^2g^{-1}, which might lead to enhanced electrochemical property [35]. BJH analysis further illustrated that the obtained Cu-rGO nanohybrid has a mesoporous distribution with a pore radius of about 1.67 nm (Figure 8b). The porous characteristics of Cu-rGO nanohybrid are beneficial to the migration of ions and the progress of the Faraday reaction [35, 36].

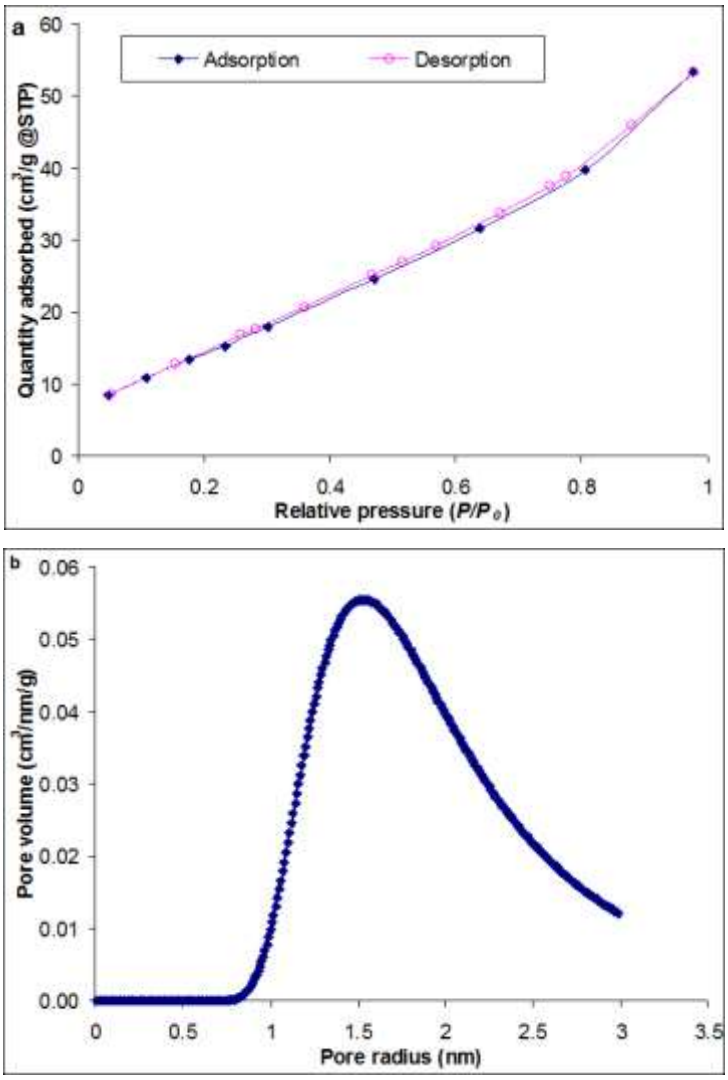

Fig. (8) : (a, b). N_2 adsorption-desorption isotherms and the pore size distribution curves of the as-prepared Cu-rGO nanohybrid.

Conclusion:

The Cu-rGO nanohybrid is successfully prepared by green synthesis via reduction effect of limon juice. The characterization tools proved the nanohybrid formation. The crystalline size calculated from Scherer equation is about 34 nm which in a good agreement with that obtained from AFM images. The BJH analysis gave a pore radius of 1.67 nm which can be used in supercapacitor applications. The crystalline strain according to Williamson-Hall equation is 0.0013. This green synthesis method demonstrates a new approach for synthesis of graphene nanohybrids materials with multifunctional applications.

Acknowledgment,

The corresponding author acknowledges grant number STDF - 34953. The authors thank Dr. G.G. Mohamed for revising the English language of the manuscript.

Reference

1. Turner, J.A., *Science*, **285**, 687 (1999).
2. Somorjai, G.A., Frei, H., Park, J.Y., *J. Am. Chem. Soc*. **131**, 16589 (2009).
3. Silva, R., Asefa, T., *Adv. Mater*. **24**, 1878 (2012).
4. Silva, R., Al-Sharab, J., Asefa, T., *Electrocatalysts. Angew. Chemie*., **124,** 7283 (2012).
5. Diego C. B., Alves Rafael, Silva Damien, Voiry Tewodros. Asefa Manish Chhowalla, *Mater. Renew Sustain Energy*, **4**, 2 (2015).
6. Geim A.K., Novoselov K.S., *Nat. Mater*. **6**, 183 (2007).
7. K. S. Park, S. D. Seo, Y. H. Jin, S. H. Lee, H. W. Shim, D. H. Lee, D.W. Kim, *Dalton Transactions*, **40**, 9498 (2011).
8. Lu Wang, Lin Chen, Yuhong Li, Hongmei Ji, Gang Yang, "Preparation of Mn_3O_4 nanoparticles at room condition for supercapacitor application", Powder Technology 235 (2013) 76-81.
9. Yang Luo, TianyeYang, Zhifang Li, Bingxin Xiao, Mingzhe Zhang, Materials Letters, **178**, 171 (2016).
10. Dadamiah PMD Shaik, P. Rosaiah, O. M. Hussain, *Materials Today Proceedings*, **3**, 64 (2016).
11. M. Mandal, D. Ghosh, K. Chattopadhyay, C. Kumar Das, *Journal Elec. Mater*. **45**, 3491 (2016).
12. Seham K. Abdel-Aal, Andrey Ionov, R. N. Mozhchil, Alim H. Naqvi, *Applied Physics A, Mat. Science and Processing* **124**, 365 (2018).
13. Seham K. Abdel-Aal, Syaed Y. Attia, Saad G. Mohamed, DOI: 10.1007/s11664-019-07305-4, Journal of Electronics Materials (2019).
14. David Dodoo-Arhin, Mopeli Fabiane, Abdulhakeem Bello, Ncholu Manyala, *Eng. Chem. Res*. **52**, 14160 (2013).
15. C. Xu, B. Xu, Y. Gu, Z. Xiong, J. Sun, X.S. Zhao, *Energ. Environ. Sci*., **6**, 1388 (2013).
16. L. Qu, C. Hu, G. Zheng, F. Zhao, H.B. Shao, Z. Zhang, N. Chen, L. Jiang, L. Qu, C. Hu, *Energ. Environ. Sci*., **7**, 3699 (2014).
17. Y. Zhou, E. Yiwen, L. Zhu, M. Qi, X. Xu, J. Bai, Z. Ren, L. Wang, *Terahertz, Carbon,* **96**, 1129 (2015).
18. L. Yang, L. Wang, M. Xing, J. Lei, J. Zhang, *Appl. Catal. B-Environ*. **180**, 106 (2016).
19. T. Xue, S. Jiang, Y. Qu, Q. Su, R. Cheng, S. Dubin, C.Y. Chiu, R. Kaner, Y. Huang, X. Duan, *Angew. Chem. Int. Edit*. **51**, 3822 (2012) .

20. M.A. Al-Daous, *Catal. Commun*., **72**, 180 (2015).
21. L. Zhao, X. Sui, J. Li, J. Zhang, L. Zhang, Z. Wang, *Catal. Commun*., **86**, 46 (2016).
22. Y. Li, W. Gao, L. Ci, C. Wang, P.M. Ajayan, *Carbon*, **48**, 1124 (2010).
23. X. Wang, P.F. Fulvio, G.A. Baker, G.M. Veith, R.R. Unocic, S.M. Mahurin, M. Chi, S. Dai, *Chem. commun*., **46**, 4487 (2010).
24. Z. Zhu, D. Su, G. Weinberg, R. Schlögl, *Nano Lett*., 4, 2255 (2004).
25. Y. Gao, D. Ma, C. Wang, J. Guan, X. Bao, *Chem. commun*., **47**, 2432 (2011).
26. R. Nie, J. Wang, L. Wang, Y. Qin, P. Chen, Z. Hou, *Carbon*, **50**, 586 (2012).
27. Xue Feng, Panpan Lv, Wei Sun, Xinyu Han, Lingfeng Gao, Gengxiu Zheng, ... , **99**, 105 (2017).
28. R.A. Sheldon, I.W.C.E. Arends, A. Dijksman, *Catal. Today*, **57**, 157 (2000).
29. K. Mori, T. Hara, T. Mizugaki, K. Ebitani, K. Kaneda, *J. Am. Chem. Soc*., **126**, 10657 (2004).
30. Y. Yu, B. Lu, X. Wang, J. Zhao, X. Wang, Q. Cai, *Chem. Eng. J.,* **162**, 738 (2010).
31. Seham K. Abdel-Aal and Ahmed S. Abdel-Rahman, *Journal of Electronic Materials*, **48**(3), 1686 (2019).
32. Y. Slimani, M.A. Almessiere, E. Hannachi, A. Baykal, A. Manikandan, M. Mumtaz, F. Ben Azzouz, *Ceramics International*, **45**, 2621 (2019).
33. M. A. Almessiere, Y. Slimani, S. Güner, J. van Leusen, A. Baykal, P. Kögerler. *Journal of Materials Science: Materials in Electronics***, 30**, 11181 (2019).
34. M. Pimenta, G. Dresselhaus, M.S. Dresselhaus, L.G. Cançado, A. Jorio, R. Saito, *Phys. Chem. Chem. Phys.,* **9**, 1276 (2007).
35. L. Xie, Z. Hu, C. Lv, G. Sun, J. Wang, Y. Li, H. He, J. Wang, K. Li, *Electrochimica Acta*, **78**, 205 (2012).
36. D. C. Marcano, D. V. Kosynkin, J. M. Berlin, A. Sinitskii,Z. Sun,A. Slesarev, L. B. Alemany,W. Lu,J. M. Tour, *ACS Nano*, **4**, 4806 (2010).